

**ORIGINAL  
RESEARCH**

G. Luthra  
A. Parihar  
K. Nath  
S. Jaiswal  
K.N. Prasad  
N. Husain  
M. Husain  
S. Singh  
S. Behari  
R.K. Gupta

# Comparative Evaluation of Fungal, Tubercular, and Pyogenic Brain Abscesses with Conventional and Diffusion MR Imaging and Proton MR Spectroscopy

**BACKGROUND AND PURPOSE:** It is difficult to differentiate the cause of brain abscesses with the use of CT and MR imaging. We did a comparative evaluation of pyogenic, tubercular, and fungal brain abscesses by using conventional, diffusion-weighted imaging (DWI), and proton MR spectroscopy (PMRS) with an aim to define the unique features that may differentiate among the pyogenic, tubercular, and fungal brain abscesses.

**MATERIALS AND METHODS:** We performed a retrospective analysis on 110 patients with surgically proved brain abscesses. Imaging studies included T2, T1, postcontrast T1, DWI, and PMRS. Apparent diffusion coefficient (ADC) of the wall and cavity of the abscesses were quantified. The morphologic, physiologic, and metabolite features of pyogenic ( $n = 91$ ), tubercular ( $n = 11$ ), and fungal ( $n = 8$ ) abscesses were compared.

**RESULTS:** The pyogenic abscesses had smooth (55/91) and lobulated (36/91) walls, whereas the tubercular abscesses had smooth (4/11), lobulated (6/11), or crenated walls (1/11) with no intracavitary projections. The fungal abscesses showed irregular walls (lobulated 4/8, crenated 4/8) with intracavitary projections (8/8). The wall as well as the cavity showed low ADC in the pyogenic and tubercular abscesses. In the fungal abscesses, the wall and projections showed low ADC (8/8); however, the cavity itself showed high ADC (8/8). PMRS showed cytosolic amino acids (89/91), acetate (25/91), and succinate (18/91) in the pyogenic abscesses, whereas lipid/lactate (11/11) was seen in the tubercular abscesses. The fungal abscesses showed lipid (4/8), lactate (7/8), amino acids (4/8), and multiple peaks between 3.6 and 3.8 ppm assigned to trehalose (5/8).

**CONCLUSION:** Based on the morphologic, ADC, and metabolite information, it may be possible to differentiate among the pyogenic, tubercular, and fungal brain abscesses.

Pyogenic abscesses of hematogenous origin are solitary in more than 50% of cases and are usually located at the gray-white matter junction in the distribution of the anterior or middle cerebral arteries. On unenhanced MR images, mature pyogenic abscesses show an isointense-to-slightly hyperintense rim on T1-weighted images and are hypointense on T2-weighted images. The ring enhancement on postcontrast images is usually thin, smooth, and often thinner along the medial margin. Daughter abscesses may be seen along the medial wall of the parent abscess. Tubercular abscesses are similar to bacterial abscesses in appearance in that they can be single or multiple, often being multiloculated. These abscesses have smooth walls with regular thickness.<sup>1</sup>

Fungal abscesses appear as solid or ring-enhancing lesions in patients who are immunocompetent.<sup>2</sup> In patients who are immunocompromised, MR imaging shows patchy or punctate T2 hyperintensity with frequently absent enhancement on postcontrast images.<sup>2,3</sup> Conventional MR imaging shows similar features in the pyogenic, tubercular, and fungal abscesses

and lacks specificity with respect to the identification of the offending microorganisms.<sup>1,2,4</sup>

In recent years, there has been an effort to characterize the etiologic agents on the basis of diffusion-weighted imaging (DWI), magnetization transfer (MT), and in vivo proton MR spectroscopy (PMRS).<sup>5-10</sup> On DWI, low ADC has been found in fungal and tubercular abscesses similar to pyogenic abscesses.<sup>3,8</sup> Tuberculous brain abscesses exhibit significantly lower MT ratios compared with those of pyogenic abscesses, with no evidence of amino acids on in vivo PMRS – a spectral hallmark of the pyogenic abscess.<sup>4,10</sup> Fungal lesions are known to show lipids (1.2–1.3 ppm), lactate (1.3 ppm), alanine (1.5 ppm), acetate (1.9 ppm), succinate (2.4 ppm), choline (3.2 ppm), and unidentified resonance at 3.8 ppm.<sup>6,11,12</sup>

In the present study, we did a comparative evaluation of pyogenic, tubercular, and fungal brain abscesses with conventional and diffusion MR imaging, and PMRS, with an aim to facilitate an early preoperative etiologic diagnosis of brain abscess.

## Materials and Methods

### Subjects

We performed a retrospective study on 110 patients referred to our tertiary care hospital for 4 years. These patients presented to us with varied clinical features such as fever, headache, and/or mass lesion, with signs and symptoms localized to the topographic location of the lesion. There were 88 male and 22 female patients with an age range between 3 and 55 years old (mean age, 31 years). We performed all

Received September 26, 2006; accepted after revision December 11.

From the Departments of Radiodiagnosis (G.L., A.P., K.N., R.K.G.), Neurosurgery (S.J., S.B.), and Microbiology (K.N.P.), Sanjay Gandhi Postgraduate Institute of Medical Sciences, Lucknow, India; and the Departments of Pathology (N.H.) and Neurosurgery (M.H., S.S.), King George Medical University, Lucknow, India.

Address correspondence to Rakesh K. Gupta, MD, MR Section, Department of Radiodiagnosis, Sanjay Gandhi Postgraduate Institute of Medical Sciences, Raebareilly Rd, Lucknow 226 014, India; e-mail: rgupta@saggi.ac.in

DOI 10.3174/ajnr.A0548

**Table 1: Summary of the mean and SD of ADC values in the walls and cavities of the 3 different types of brain abscess**

Type of Abscess	Apparent Diffusion Coefficient (mean ± SD) × 10 <sup>-3</sup> mm <sup>2</sup> /s*		
	Wall	Restricted Portion of Cavity	Nonrestricted Portion of Cavity
Pyogenic (n = 91)	0.79 ± 0.19	0.73 ± 0.18	1.32 ± 0.41
Tubercular (n = 11)	0.83 ± 0.34	0.66 ± 0.23	1.61 ± 0.42
Fungal (n = 8)	0.81 ± 0.22	0.50 ± 0.05	1.50 ± 0.42
P values	P = 0.35†§	P = 0.23†§	P = 0.90†§
	P = 0.77†§	P = 0.01†§	P = 0.41†§
	P = 0.36††	P = 0.51††	P = 0.39††

\* The mean ADC of normal-appearing white matter in our study was  $0.74 \pm 0.07 \times 10^{-3} \text{ mm}^2/\text{s}$ .

† Pyogenic abscess.

‡ Tubercular abscess.

§ Fungal abscess.

studies within the guidelines of the Institutional Review Board. Informed consent was taken from the patients or their relatives for the study. In 110 patients with organism-proved abscesses (based on microscopic examination of culture and histopathologic examination of surgically aspirated or excised lesions), there were 91 pyogenic, 11 tubercular, and 8 fungal abscesses without underlying sinonasal infection. We studied conventional MR imaging, DWI, and PMRS features in these patients. In patients with multiple lesions, we did an analysis of the imaging features of the largest abscess that was aspirated or excised. None of the patients with pyogenic and tubercular abscesses were immunocompromised. The following predisposing factors were present in the patients who had pyogenic abscesses: otitis media (n = 30), sinusitis (n = 10), septicemia (n = 9), dental caries (n = 7), posttraumatic (n = 6), congenital heart disease (n = 5), postoperative (n = 3), and postmeningitis (n = 2). In the remaining 19 patients with a pyogenic brain abscess, no predisposing factor could be identified. In only 3 patients with tubercular abscess, findings consistent with pulmonary tuberculosis were seen on chest radiograph. Four patients with a fungal brain abscess had known immune suppression: 2 were renal transplant recipients on immunosuppressant drugs, 1 had non-Hodgkin lymphoma and was undergoing treatment, and 1 had diabetes. The remaining 4 patients were immunocompetent. The histopathologic features of the wall of the abscess were available in 5 pyogenic, 6 tubercular, and 1 fungal.

### MR Imaging

We performing the imaging on a 1.5T MR system (Signa; GE Medical Systems, Milwaukee, Wis) equipped with an actively shielded whole-body magnetic field gradient set (allowing up to 33 mT/m) by using a quadrature birdcage receive and transmit radio-frequency head coil. The routine imaging studies included fast spin-echo (FSE) T2-weighted (TR, 4900 ms; TE, 85 ms; NEX, 3), and T1-weighted (TR, 650 ms; TE, 14 ms; NEX, 2) with a matrix size of 256 × 256; FOV, 24 × 24 cm and no intersection gap. We performed diffusion-weighted echo-planar imaging (EPI) in the axial plane with a single-shot EPI-spin-echo (SE) pulse sequence with the following parameters: TR, 10.5 s; TE, 110 ms (minimum); FOV, 24 × 24 cm; NEX, 2; section thickness, 5 mm; no intersection gap; and a matrix size of 128 × 128 interpolated to 256 × 256. Diffusion-sensitizing gradients were applied sequentially along the 3 orthogonal directions with a diffusion sensitivity of b = 0 and 1000 s/mm<sup>2</sup>. Ramp sampling was switched on to reduce the echo spacing, thereby minimizing the geometric distortion. In vivo PMRS was performed with water-suppressed localized single-voxel SE sequence with TR, 3000 ms; TE, 144 ms; NEX, 8; and a voxel size of 2–3 mL, depending on the size of the lesion. We ensured voxel placement within the cavity of the lesion to avoid contamination from the surrounding brain parenchyma as well

as the wall of the cavity. After global shimming, voxel shimming was performed, and a full width at half maximum of 4–6 Hz was achieved in all the cases. Only the long TE technique was used, because it has been observed that the metabolites in brain abscesses have intermediate-to-long T2 values and are well assigned at a TE of 144 ms.<sup>9,10,13</sup>

### Qualitative Analysis

The size, presence of satellite lesions, and multiplicity of the abscesses were noted. A small lesion in the vicinity of a larger lesion in the same section was considered a satellite lesion. The lesions were considered multiple when there were more than 1, either in the same section or anyplace else in the brain parenchyma. The morphologic features of the lesions were analyzed on T2-weighted images on the basis of their outer margins, the presence of projections from the wall, and debris (a T2 isointense or hypointense area separate from the wall). The outer margin of the wall was classified as smooth (no angulations), lobulated (few obtuse angles), or crenated (multiple acute angles) depending on the shape of the margins. Debris was considered to be present when the ADC of the T2 hypointense foci in the cavity was more than  $0.90 \pm 0.13 \times 10^{-3} \text{ mm}^2/\text{s}$ .<sup>9,13</sup> A lesion with an ADC of less than  $0.90 \pm 0.13 \times 10^{-3} \text{ mm}^2/\text{s}$  was considered the result of increased cellularity (inflammatory cells and offending organism).<sup>13</sup>

### Quantitative Analysis

We calculated the ADC of the walls and cavities of the abscesses along with comparative evaluation of the pyogenic, tubercular, and fungal types, as shown in Table 1. We generated an ADC map pixel by pixel by using the following formula:

$$\text{ADC} = b^{-1} \ln (S_0/S)$$

where S<sub>0</sub> and S represent the signal intensities of the image without and with diffusion-weighted gradients. We selected the region of interest of the wall (2 × 2 to 4 × 4 pixels) by using the freehand technique. The wall was defined on postcontrast SE T1-weighted images; it was then registered on the DWI. We quantified the mean ADC values from the cavity of the pyogenic, tubercular, and fungal abscesses in all the sections from the restricted and nonrestricted portions of the cavity (Table 1). When the DWI images showed hyperintensity with ADC values less than  $0.90 \pm 0.13 \times 10^{-3} \text{ mm}^2/\text{s}$ , the portions were considered restricted; for higher values, the portions were considered nonrestricted.<sup>9,13</sup>

We analyzed the PMRS data by using standard Java-based MR user interface software (jMRUI Europe project, Leuven, Belgium). Assignments of the various resonances were based on the literature; the signal intensity from lactate at 1.33 ppm was used as an internal reference of chemical shift.<sup>14</sup>

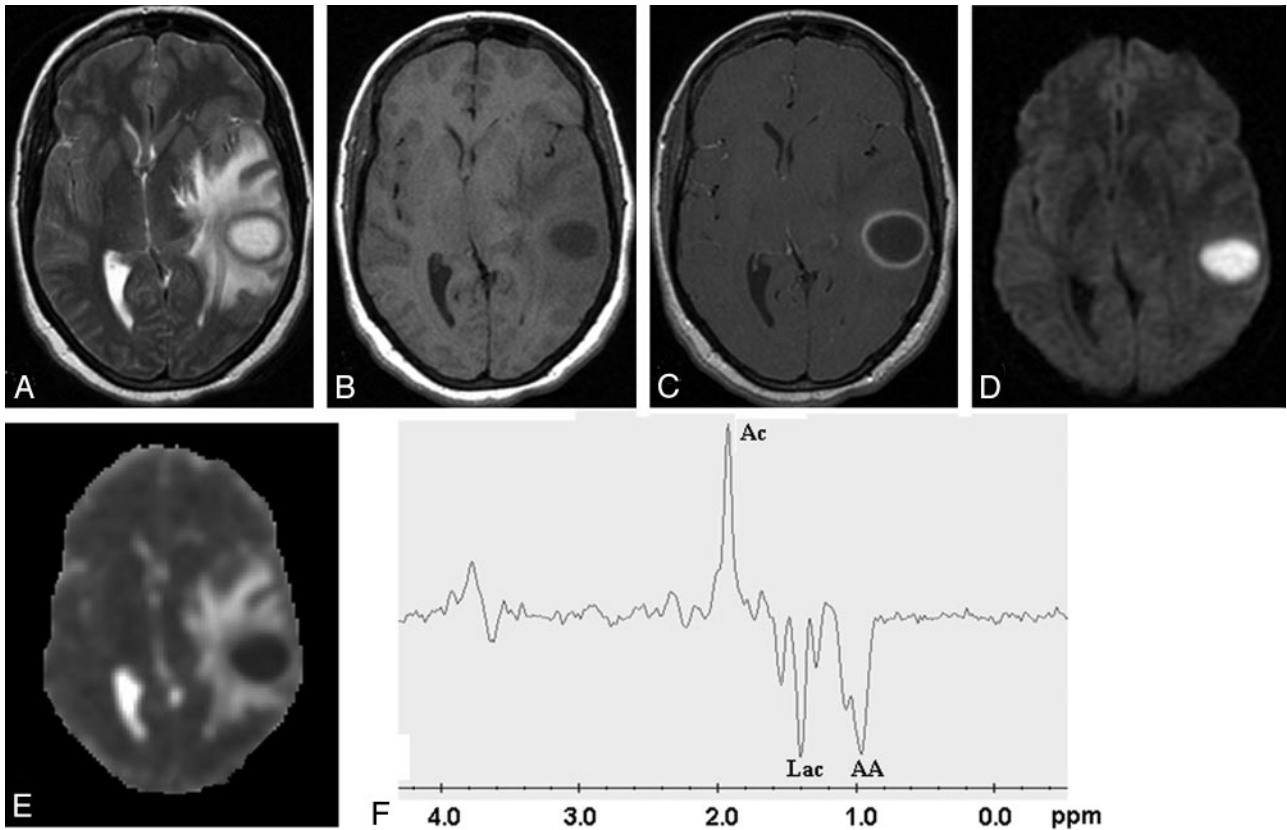


**Fig 1.** Pyogenic abscess in the left temporal lobe of a 31-year-old woman.

Axial T2-weighted image (A) shows a well-defined hyperintense lesion with hypointense wall that appears hypointense on axial T1-weighted image (B) with isointense wall. On postcontrast T1-weighted image (C), it shows ring enhancement. Diffusion-weighted image shows homogeneous hyperintensity in the cavity (D) with low ADC ( $0.63 \times 10^{-3} \text{ mm}^2/\text{s}$ ) (E). PMRS from the center of the lesion with a voxel size of 2.4 mL shows amino acids (AA, 0.9 ppm), lactate (Lac, 1.3 ppm), and acetate (Ac, 1.9 ppm) (F). Culture from pus grew *Bacteroides* species.

### Statistical Analysis

We performed a 2-tailed Student independent *t* test by using the SPSS version 12.0 (SPSS, Chicago, Ill). We computed *P* values for mean signal intensities from the wall of the abscess, and the restricted and nonrestricted portions of the cavity in the pyogenic, tubercular, and fungal types to look for any significant differences. A *P* value of less than .05 was regarded as statistically significant.

### Results

#### Clinical Data

In our patients, the most common symptom was headache ( $n = 87$ ), followed by fever ( $n = 63$ ), altered sensorium ( $n = 35$ ), hemiparesis ( $n = 12$ ), seizures ( $n = 11$ ), paresthesia or hypoesthesia ( $n = 11$ ), visual disturbance ( $n = 9$ ), and cerebellar signs ( $n = 7$ ). Seventy-six pyogenic abscesses were solitary: frontal ( $n = 21$ ), temporal ( $n = 22$ ), parietooccipital ( $n = 19$ ), parietal ( $n = 8$ ), and cerebellar ( $n = 6$ ). The remaining 15 pyogenic abscesses were in multiple locations with 9 satellite lesions (9.8%). Six tubercular abscesses were solitary: frontal ( $n = 1$ ), parietal ( $n = 2$ ), basal ganglia ( $n = 1$ ), cerebellar ( $n = 1$ ), occipital ( $n = 1$ ). Five tubercular abscesses were in multiple locations with 3 satellite lesions (27.2%).

Of the 91 pyogenic abscesses, 23 were culture sterile, 68 were culture positive. The gram-positive organisms included *Streptococcus viridans* ( $n = 19$ ), *Staphylococcus aureus* ( $n = 10$ ), *Enterobacter faecalis* ( $n = 5$ ), *Nocardia* ( $n = 4$ ), *Peptostreptococcus* ( $n = 6$ ), *Listeria monocytogenes* ( $n = 1$ ), *Corynebacte-*

*rium* species ( $n = 1$ ), *Propionibacterium* species ( $n = 1$ ), and *Eubacterium* ( $n = 1$ ). The gram-negative organisms included *Escherichia coli* ( $n = 5$ ), *Klebsiella pneumoniae* ( $n = 2$ ), *Pseudomonas* ( $n = 3$ ), *Proteus mirabilis* ( $n = 1$ ), *Eikenella corrodens* ( $n = 1$ ), *Bacteroides fragilis* ( $n = 5$ ), *Bacteroides* species ( $n = 1$ ), and *Fusobacterium* ( $n = 2$ ). There were 5 solitary fungal abscesses: frontal ( $n = 2$ ), frontoparietal ( $n = 1$ ), parietooccipital ( $n = 1$ ), and basal ganglia ( $n = 1$ ); the remaining 3 were in multiple locations with 1 satellite lesion (12.5%).

Of the 8 fungal abscesses, 7 were of filamentous fungi: the organisms *Aspergillus flavus* ( $n = 3$ ) and *A fumigatus* ( $n = 2$ ), and the infections mucormycosis ( $n = 1$ ) and zygomycosis ( $n = 1$ ). One abscess was caused by a dematiaceous, or phaeomycotic, fungal infection ( $n = 1$ ). All 11 tubercular abscesses grew *Mycobacterium tuberculosis* on culture.

#### Conventional MR Features

The pyogenic abscesses ranged in size from 3–70 mL, with most of them being 8–17 mL. The tubercular abscesses ranged in size from 3–20 mL, most being 3–11 mL. The fungal abscesses ranged in size from 5–47 mL, most being 11–17 mL.

All the pyogenic, tubercular, and fungal abscesses were hypointense on T1-weighted and hyperintense on T2-weighted images and showed well-defined rim enhancement on post-contrast images. In the walls of the pyogenic abscesses, the outer margin was smooth ( $n = 55$ , 60.4%) or lobulated ( $n = 36$ , 39.6%) (Fig 1). In the tubercular abscesses, it was smooth

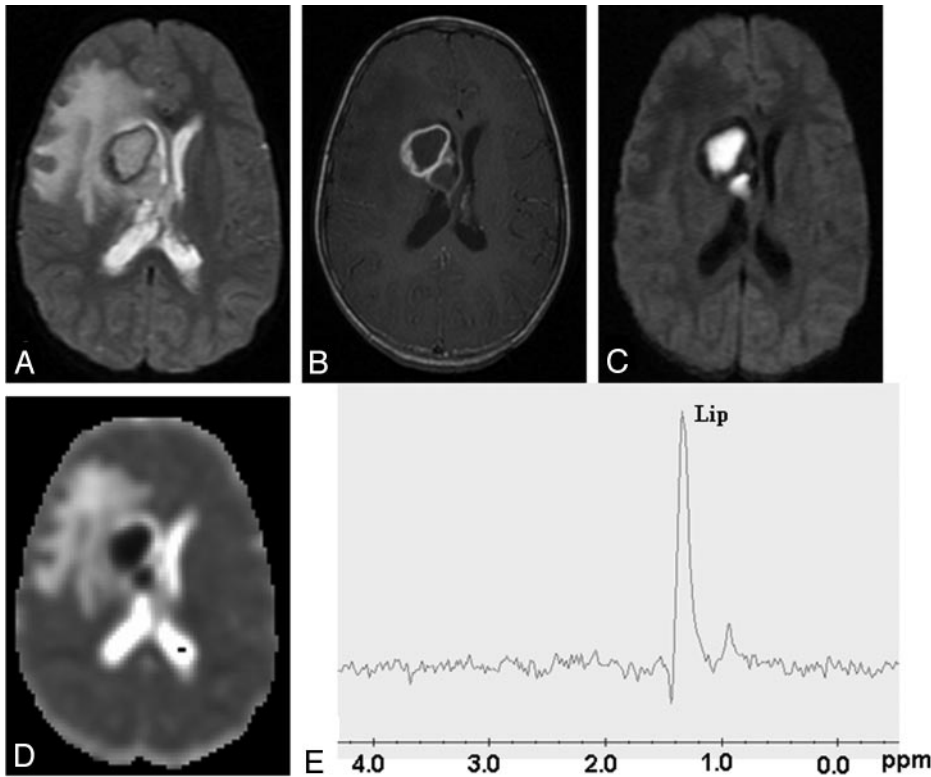


**Fig 2.** Tubercular abscess in the right basal ganglia of a 25-year-old woman.

A well-defined hyperintense lesion is seen with a hypointense wall on axial T2-weighted image (A), which shows ring enhancement on post-contrast T1-weighted image (B). Diffusion-weighted image shows homogeneous hyperintensity in the cavity (C) with low ADC ( $0.54 \times 10^{-3} \text{ mm}^2/\text{s}$ ) (D). PMRS from the center of the lesion with a voxel size of 2 mL shows predominant lipid peak (Lip, 1.3 ppm) (E). Culture from pus shows the presence of *Mycobacterium tuberculosis*.

( $n = 4, 36.3\%$ ), lobulated ( $n = 6, 54.5\%$ ), and crenated ( $n = 1, 9.1\%$ ) (Fig 2). In the fungal abscesses, the margin was crenated ( $n = 4, 50\%$ ) and lobulated ( $n = 4, 50\%$ ) (Fig 3, 4). Satellite lesions were seen in 9 (9.8%) pyogenic, 1 (12.5%) fungal, and 3 (27.2%) tubercular abscesses. In each of the 8 fungal abscesses, the intracavitary projections from the wall of the abscess were isointense to hypointense on T1-weighted and hypointense on T2-weighted images. No projections were seen in the pyogenic or tubercular abscesses. Debris within the lesion was seen in 36 (39.5%) pyogenic and 4 (36.3%) tubercular abscesses. The projections in all fungal abscesses were isointense to hypointense on T2-weighted and isointense on T1-weighted images. Contrast enhancement was seen only in the wall of the fungal abscess, with no enhancement of the projections.

#### Diffusion-Weighted Imaging

The mean ADC of normal-appearing white matter in our study was  $0.74 \pm 0.07 \times 10^{-3} \text{ mm}^2/\text{s}$ . Mean ADC values of the wall, and restricted and nonrestricted portions of the pyogenic abscesses were  $0.79 \pm 0.19$ ,  $0.73 \pm 0.18$ , and  $1.32 \pm 0.41 \times 10^{-3} \text{ mm}^2/\text{s}$ , respectively (Table 1). Likewise, in the tubercular abscesses, the ADC values of the wall, and restricted and nonrestricted portions were  $0.83 \pm 0.34$ ,  $0.66 \pm 0.23$ , and  $1.61 \pm 0.42 \times 10^{-3} \text{ mm}^2/\text{s}$  respectively. In the fungal abscesses, the values were  $0.81 \pm 0.22$ ,  $0.50 \pm 0.05$ , and  $1.50 \pm 0.42 \times 10^{-3} \text{ mm}^2/\text{s}$ , respectively. The fungal abscesses showed restriction of diffusion in the projections and the wall, whereas the rest of the abscess core showed no restriction of diffusion. There was a significantly higher mean ADC value of the wall compared with the intracavitary projections in the fungal abscesses ( $P < .001$ ).

Comparative analysis of ADC values from the walls of

the pyogenic, tubercular, and fungal abscesses showed no significant statistical difference, as shown in Table 1. The ADC values of the restricted and nonrestricted portions of the abscesses were also compared, and significantly low ADC values were observed in the restricted portions of the fungal abscesses compared with the pyogenic group ( $P = .01$ ). Although the ADC values in the restricted portion of the fungal abscesses were lower than that of the tubercular abscesses, they did not reach the level of statistical significance ( $P = .23$ ). The difference in the ADC values of the nonrestricted portions of the pyogenic and tubercular ( $P = .39$ ), pyogenic and fungal ( $P = .41$ ), and tubercular and fungal ( $P = .90$ ) abscesses was not significant.

#### In Vivo Proton MR Spectroscopy

Various metabolites observed from the 3 different types of abscesses are summarized in Table 2. In vivo PMRS showed cytosolic amino acids (0.9 ppm,  $n = 89/91$ ) in the pyogenic abscesses along with lactate (1.3 ppm,  $n = 46/91$ ), lipid with lactate (1.3 ppm,  $n = 45/91$ ), acetate (1.92 ppm,  $n = 25/91$ ), and succinate (2.4 ppm,  $n = 18/91$ ) (Fig 1). The tubercular lesions had lipid peaks in all 11 abscesses at 1.3 ppm (Fig 2). Four fungal abscesses showed amino acids (0.9 ppm) and lactate (1.3 ppm), 3 showed lipid with lactate (1.3 ppm), and 1 fungal abscess showed lipid alone (1.3 ppm). Multiple signals were also seen between 3.6 and 3.8 ppm in 5 of 8 lesions (Fig 4); these peaks were assigned to trehalose present in the fungal wall, as reported in the literature.<sup>12</sup>

#### Discussion

##### Conventional MR Imaging Features

Pyogenic abscesses evolve through the early cerebritis, late cerebritis, early capsular, and late capsular stages of formation.<sup>1</sup> In the cerebritis stage, pyogenic abscesses are seen as T1 hypointense and T2 hyperintense areas with minimal or nonhomogenous enhancement.<sup>1</sup> Tuberculous cerebritis is seen as an ill-defined, hypoattenuated area with gyral enhancement.<sup>15</sup> Fungal cerebritis lesions are nonenhancing and are usually located in the basal ganglia and deep white matter.<sup>3</sup> Peripheral rim enhancement has been reported in mature pyogenic and fungal abscesses.<sup>1,3</sup> On the basis of conventional MR findings,

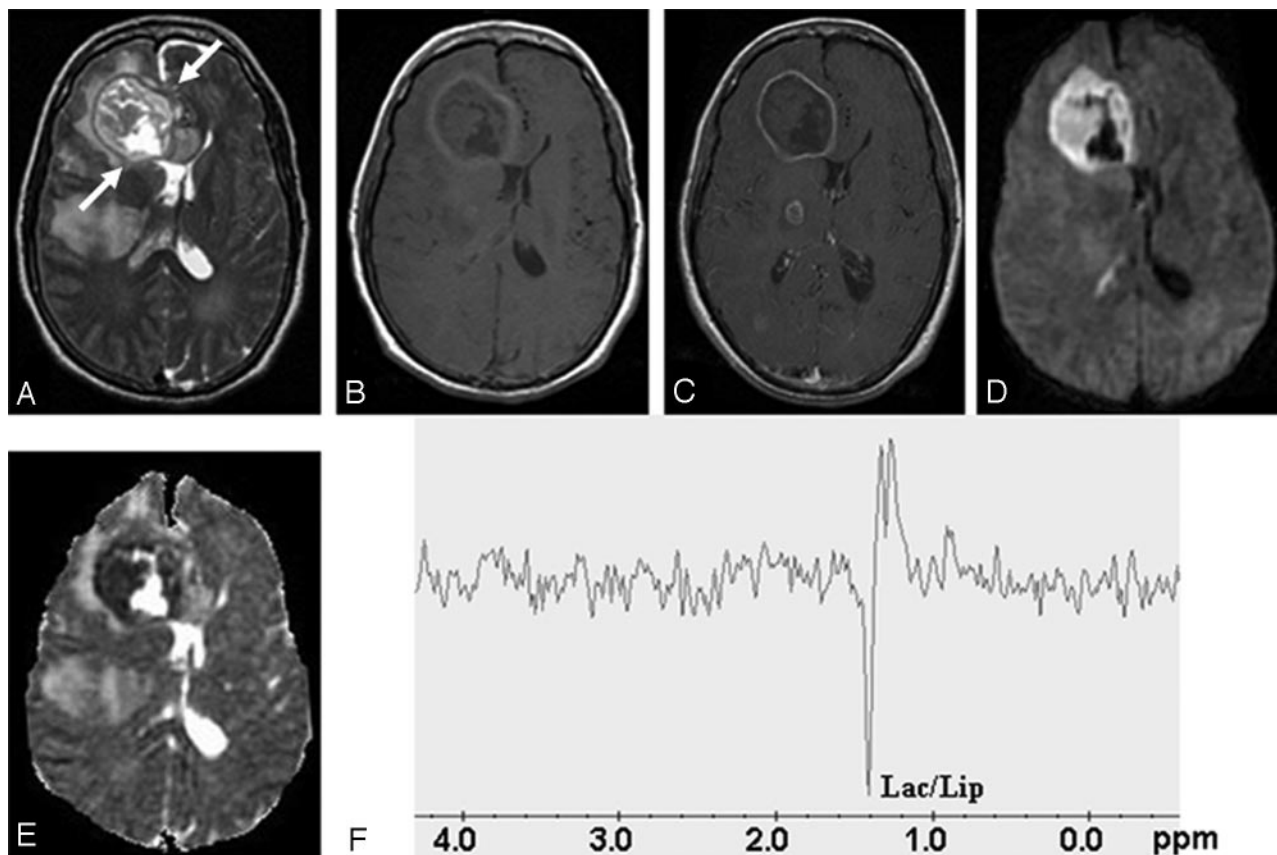


**Fig 3.** Fungal abscess in the frontal lobe of a 39-year-old man with non-Hodgkin lymphoma on treatment.

Axial T2-weighted image (A) shows a well-defined heterointense lesion in the right frontal lobe with an irregular hypointense wall. Hypointense projections attached to the wall are well demonstrated. White arrows show the crenated margin of the fungal wall. Axial T1-weighted image (B) shows a hypointense core with isointense intracavitary projections. Postcontrast axial T1-weighted image (C) shows peripheral enhancement of the wall with no enhancement of intracavitary projections. Note the presence of 2 more enhancing lesions in the right thalamus and right occipital regions, which are better seen in adjoining sections. Diffusion-weighted image (D) shows hyperintensity in the projections with hypointensity in the cavity. On an ADC map (E), intracavitary projections show low ADC ( $0.46 \times 10^{-3} \text{ mm}^2/\text{s}$ ) with high ADC in the cavity ( $2.22 \times 10^{-3} \text{ mm}^2/\text{s}$ ). PMRS (F) obtained with a voxel size of 2 mL shows lactate along with lipid (Lac/Lip, 1.3 ppm). Culture from pus grew *Aspergillus flavus*.

**Table 2: Summary of the metabolites observed in the 3 types of brain abscesses studied**

Type of Abscess	Metabolite*						
	Amino Acid (0.9 ppm)	Lipid (1.3 ppm)	Lactate (1.3 ppm)	Lipid + Lactate	Acetate (1.9 ppm)	Succinate (2.4 ppm)	(3.6–3.8 ppm)†
Pyogenic	89	–	46	45	25	18	–
Tubercular	–	9	–	2	–	–	–
Fungal	4	1	4	3	–	–	5

\* The figures indicate the number of abscesses that showed the presence of a particular metabolite.

† Multiple peaks between 3.6 and 3.8 were assigned to trehalose, as reported in the literature.<sup>12</sup>

it is not possible to characterize the cause of brain abscess in both cerebritis and abscess stages of formation<sup>1-4</sup>. All the abscesses in our series were predominantly hypointense on T1 and hyperintense on T2-weighted images with well-defined peripheral rim enhancement and could not be etiologically characterized on conventional MR imaging on the basis of the known features. Imaging features in all the cases in the present study seemed to be in the late capsular stage.

In 100% of the pyogenic and 90.9% of the tubercular abscesses, the outer margin of the wall was either smooth or lobulated – in contrast to the fungal lesions, which had a crenated wall in half of the abscesses. All the fungal abscesses showed intracavitary projections directed centrally from the wall without any contrast enhancement in these projections. These projections were not seen in the other types and seemed to be a distinguishing

feature of a fungal cause on conventional MR imaging. A review of the literature revealed only 1 study<sup>5</sup> of conventional MR findings in fungal brain abscess. In the study, Ashdown et al<sup>5</sup> described 4 cases of fungal abscesses in patients who were immunocompromised; these abscesses had an irregular T2 hypointense rim that showed postcontrast enhancement.

#### Diffusion-Weighted Imaging

We found restriction on DWI with low ADC values ( $0.72 \pm 0.17 \times 10^{-3} \text{ mm}^2/\text{s}$ ) in the cavity of the pyogenic abscesses similar to findings reported previously.<sup>16-19</sup> Low ADC values between  $0.28$  and  $0.70 \times 10^{-3} \text{ mm}^2/\text{s}$  have been reported in bacterial abscesses and ascribed to the presence of intact inflammatory cells and bacteria that collectively impede the microscopic motion of water molecules.<sup>13</sup> Low ADC has also been

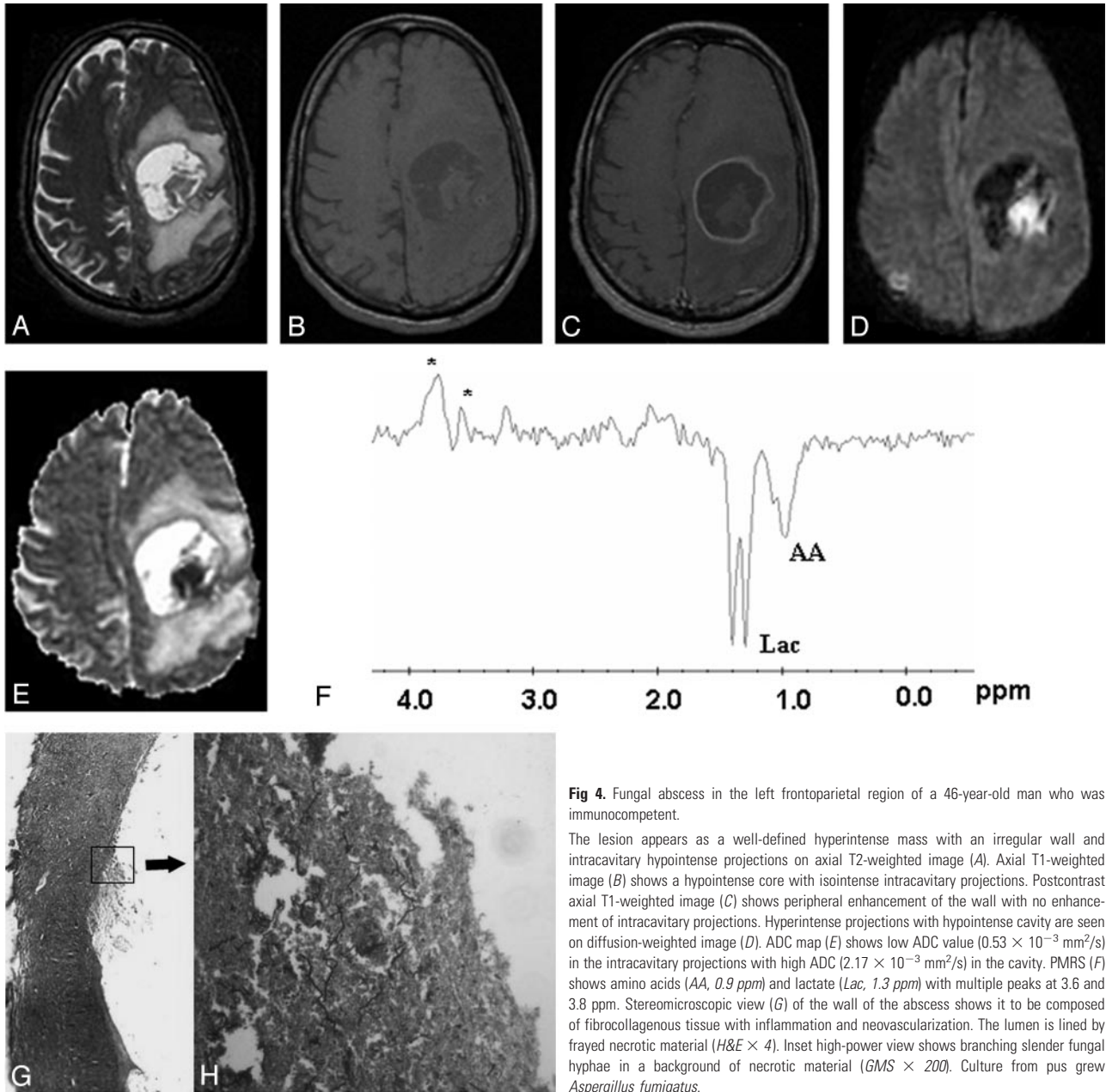


**Fig 4.** Fungal abscess in the left frontoparietal region of a 46-year-old man who was immunocompetent.

The lesion appears as a well-defined hyperintense mass with an irregular wall and intracavitary hypointense projections on axial T2-weighted image (A). Axial T1-weighted image (B) shows a hypointense core with isointense intracavitary projections. Postcontrast axial T1-weighted image (C) shows peripheral enhancement of the wall with no enhancement of intracavitary projections. Hyperintense projections with hypointense cavity are seen on diffusion-weighted image (D). ADC map (E) shows low ADC value ( $0.53 \times 10^{-3} \text{ mm}^2/\text{s}$ ) in the intracavitary projections with high ADC ( $2.17 \times 10^{-3} \text{ mm}^2/\text{s}$ ) in the cavity. PMRS (F) shows amino acids (AA, 0.9 ppm) and lactate (Lac, 1.3 ppm) with multiple peaks at 3.6 and 3.8 ppm. Stereomicroscopic view (G) of the wall of the abscess shows it to be composed of fibrocollagenous tissue with inflammation and neovascularization. The lumen is lined by frayed necrotic material (H&E  $\times 4$ ). Inset high-power view shows branching slender fungal hyphae in a background of necrotic material (GMS  $\times 200$ ). Culture from pus grew *Aspergillus fumigatus*.

observed in tubercular abscesses, which is consistent with our observations and is considered to be the result of the presence of intact inflammatory cells in the pus.<sup>8,13</sup> High ADC in the cavity of a pyogenic abscess has been found after surgical drainage of pus and/or on medications and has been shown to correlate with good therapeutic response.<sup>9,20</sup>

Low ADC in fungal cerebritis and fungal abscess has also been described previously and, thus, at first glance does not seem to differentiate between the fungal and nonfungal causes of brain abscess.<sup>3,21</sup> However, the analysis of DWI images and ADC values showed restricted diffusion in the projections and wall of the fungal abscess. The rest of the core of the abscess showed no restricted diffusion, whereas the pyogenic and tubercular group showed restricted diffusion in the core of the cavity. The restricted portion correlated with isointense-to-hypointense projections in the fungal group, in contrast to the T2 hyperintense core in the pyogenic and tubercular groups.

ADC values in the restricted portion seemed to be lower in the fungal abscess group and showed a significant difference compared with the pyogenic group ( $P = .01$ ).

Heterogeneity of diffusion in fungal infection has been described by Gaviani et al.<sup>3</sup> They described areas of increased and decreased diffusion in 2 fungal abscesses in the cerebritis stage and 1 in the early capsular stage. As opposed to our observation, their 6 cases of the late capsular stage showed uniform restriction of diffusion. It is likely that the abscesses in the late capsular stage in their series had the cavity full of inflammatory cells along with fungal hyphae that presented as uniform restriction of diffusion.

#### Proton MR Spectroscopy

PMRS in the pyogenic group revealed the presence of amino acids in 89 of 91 abscesses along with lipid and lactate, and acetate and succinate and is consistent with the literature.<sup>10</sup> Pyogenic brain abscesses contain large amounts of neutrophils

and proteins, which are released in the necrotic cavity. The breakdown of the neutrophils results in the release of a large amount of proteolytic enzymes that hydrolyze the proteins into amino acids at 0.9 ppm, as seen in *in vivo* PMRS in pyogenic brain abscesses.<sup>10</sup> Absence of amino acids in 2 of the pyogenic abscesses, which grew *S aureus* on culture, has been comprehensively shown in animal models of *S aureus* and in vivo human studies.<sup>22</sup> *In vivo* demonstration of amino acid resonance in a case of mucormycosis is in support of our finding in 4 of 8 fungal abscesses and may be because of the existence of a proteolytic mechanism similar to that in pyogenic abscesses.<sup>11</sup> Acetate and succinate are the end products of heterolactic and homolactic fermentation and were seen only in pyogenic abscesses, though occurrence in a single case of cerebral mucormycosis has been shown.<sup>6</sup> Lactate or lactate with lipid may be seen in any of the 3 causes. However, the presence of lipid peak with absence of other metabolites such as amino acids, succinate, and acetate should suggest a tubercular cause in most patients.

*In vivo* PMRS of fungal abscesses showed cytosolic amino acids and lipid and lactate, which was not remarkably different from that of pyogenic abscesses until the presence of multiple signals seen between 3.6 and 3.8 ppm assigned to the disaccharide trehalose in 5 of 8 fungal abscesses was taken into account. Such signals have been reported in the wall of cryptococcomas<sup>12</sup> and cerebral mucormycosis.<sup>6</sup> The absence of these resonances in the 3 fungal abscesses could be the result of lower concentrations of these metabolites, which are below the sensitivity of *in vivo* PMRS on the 1.5T MR imaging system.

Intracavitary projections seemed to be characteristic of fungal abscesses and could be confirmed as fungal hyphae on histopathologic examination from the wall of the excised abscess (Fig 4G). *In vitro* studies of the fungal colony have shown accrual of paramagnetic elements with growth of hyphae resulting in increased magnetic susceptibility effects and decreased signal intensity on T2-weighted images.<sup>23</sup> The neovascularity and leakage of contrast media as a result of disruption of the blood-brain barrier into the interstitial tissue explain the contrast enhancement of the abscess wall. However, nonenhancement of these projections on postcontrast study suggests poor vascularity in these structures. It is possible that the projections represent zones of active proliferation of hyphae to avoid host defense mechanisms in the innermost part of the thick granulation tissue of the abscess wall.<sup>24</sup> The presence of irregular projections into the core of the abscess with ADC values significantly lesser than those of the wall is probably because of the presence of fungal elements containing paramagnetic substances in the fungal tissue along with inflammatory cells.<sup>25,26</sup> The presence of debris in the pyogenic abscesses observed on T2-weighted images showed a high ADC value and could be readily differentiated from the projections with a low ADC in the fungal abscess.

## Conclusion

Pyogenic and tubercular abscesses may be differentiated by their unique metabolite pattern with recognition of amino acids, acetate, and succinate in pyogenic abscesses and lipid peak in tubercular abscesses. Fungal abscesses can be differentiated from nonfungal abscesses by a combination of the conventional, DWI, and PMRS features. A ring-enhancing T2 heterointense lesion with irregular walls and irregular projections

into the cavity with low ADC and no contrast enhancement of these projections carries a high probability of being a fungal abscess. The identification of multiple signals seen between 3.6 and 3.8 ppm may add further to the diagnostic confidence.

## References

- Whiteman MLH, Bowen BC, Post MJD, et al. **Intracranial infection.** In: Atlas SW, ed. *Magnetic Resonance Imaging of the Brain and Spine*. 3rd ed. Philadelphia: Lippincott Williams and Wilkins; 2002:1099–177
- Kastrup O, Wanke I, Maschke M. **Neuroimaging of infections.** *NeuroRx* 2005;2:324–32
- Gaviani P, Schwartz RB, Hedley-Whyte ET, et al. **Diffusion-weighted imaging of fungal cerebral infection.** *AJNR Am J Neuroradiol* 2005;26:1115–121
- Gupta RK, Vatsal DK, Husain N, et al. **Differentiation of tuberculous from pyogenic brain abscesses with *in vivo* proton MR spectroscopy and magnetization transfer MR imaging.** *AJNR Am J Neuroradiol* 2001;22:1503–09
- Ashdown BC, Tien RD, Felsberg GJ. **Aspergillosis of the brain and paranasal sinuses in immunocompromised patients: CT and MR imaging findings.** *AJR Am J Roentgenol* 1994;162:155–59
- Siegel JA, Cacayorinb ED, Nassif AS, et al. **Cerebral mucormycosis: proton MR spectroscopy and MR imaging.** *Magn Reson Imaging* 2000;18:915–20
- Faria AV, Dabus GC, Zanardi VA, et al. **Proton magnetic resonance spectroscopy and magnetic resonance imaging findings in a patient with central nervous system paracoccidioidomycosis.** *J Neuroimaging* 2004;14:377–79
- Gupta RK, Prakash M, Mishra AM, et al. **Role of diffusion weighted imaging in differentiation of intracranial tuberculoma and tuberculous abscess from cysticercus granulomas—a report of more than 100 lesions.** *Eur J Radiol* 2005;55:384–92
- Mishra AM, Gupta RK, Jaggi RS, et al. **Role of diffusion-weighted imaging and *in vivo* proton magnetic resonance spectroscopy in the differential diagnosis of ring-enhancing intracranial cystic mass lesions.** *J Comput Assist Tomogr* 2004;28:540–47
- Garg M, Gupta RK, Husain M, et al. **Brain abscesses: etiologic categorization with *in vivo* proton MR spectroscopy.** *Radiology* 2004;230:519–27
- Garg M, Gupta RK. **MR spectroscopy in intracranial infection.** In: Gillard JH, Waldman AD, Barker PB, eds. *Clinical MR Neuroimaging: Diffusion, Perfusion and Spectroscopy*. Cambridge, UK: Cambridge University Press; 2005:380–406
- Himmelreich U, Dzendrowskyj TE, Allen C, et al. **Cryptococcomas distinguished from gliomas with MR spectroscopy: an experimental rat and cell culture study.** *Radiology* 2001;220:122–28
- Mishra AM, Gupta RK, Saksena S, et al. **Biological correlates of diffusivity in brain abscess.** *Magn Reson Med* 2005;54:878–85
- Govindaraju V, Young K, Maudsley AA. **Proton NMR chemical shifts and coupling constants for brain metabolites.** *NMR Biomed* 2000;13:129–53
- Jenkins JR, Gupta R, Chang KH, et al. **MR imaging of central nervous system tuberculosis.** *Radiol Clin North Am* 1995;33:771–86
- Ebisu T, Tanaka C, Umeda M, et al. **Discrimination of brain abscess from necrotic or cystic tumors by diffusion-weighted echo planar imaging.** *Magn Reson Imaging* 1996;14:1113–16
- Desprechins B, Stadnik T, Koerts G, et al. **Use of diffusion-weighted MR imaging in differential diagnosis between intracerebral necrotic tumors and cerebral abscesses.** *AJNR Am J Neuroradiol* 1999;20:1252–57
- Noguchi K, Watanabe N, Nagayoshi T, et al. **Role of diffusion-weighted echoplanar MRI in distinguishing between brain abscess and tumour: a preliminary report.** *Neuroradiology* 1999;41:171–74
- Tung GA, Evangelista P, Rogg JM, et al. **Diffusion-weighted MR imaging of rim-enhancing brain masses: is markedly decreased water diffusion specific for brain abscess?** *AJR Am J Roentgenol* 2001;177:709–12
- Cartes-Zumelzu FW, Stavrou I, Castillo M, et al. **Diffusion-weighted imaging in the assessment of brain abscesses therapy.** *AJNR Am J Neuroradiol* 2004;25:1310–17
- Tung GA, Rogg JM. **Diffusion-weighted imaging of cerebritis.** *AJNR Am J Neuroradiol* 2003;24:1110–13
- Himmelreich U, Accurso R, Malik R, et al. **Identification of *Staphylococcus aureus* brain abscesses: rat and human studies with 1H MR spectroscopy.** *Radiology* 2005;236:261–70
- Fellows DW, King VD, Conturo T, et al. ***In vitro* evaluation of MR hypointensity in *Aspergillus* colonies.** *AJNR Am J Neuroradiol* 1994;15:1139–44
- Yamada K, Zoarski GH, Rothman MI, et al. **An intracranial aspergilloma with low signal on T2-weighted images corresponding to iron accumulation.** *Neuroradiology* 2001;43:559–61
- Xia Z, Nguyen BD, La Mar GN. **The use of chemical shift temperature gradients to establish the paramagnetic susceptibility tensor orientation: implication for structure determination/refinement in paramagnetic metalloproteins.** *J Biomol NMR* 2000;17:167–74
- Haris M, Gupta RK, Husain N, et al. **Measurement of DTI metrics in hemorrhagic brain lesions: possible implication in MRI interpretation.** *J Magn Reson Imaging* 2006;24:1259–68